Bayesian Treatment Of Sensory Tuning Curves

A Master's Thesis

Presented to

The Faculty of the Graduate School of Arts and Sciences
Brandeis University

Graduate Program in Biochemistry and Biophysics

Stephen D. Van Hooser, Advisor

In Partial Fulfillment
of the Requirements for the Degree
Master of Science

by

Zongting Wu

May 2024

ABSTRACT

Bayesian Treatment Of Sensory Tuning Curves

A thesis presented to the Faculty of the
Graduate School of Arts and Sciences of Brandeis University
Waltham, Massachusetts

By Zongting Wu

This study explores the efficacy of Bayesian estimation in modeling the orientational and directional selectivity of neurons in the primary visual cortex (V1), providing a profound understanding of neuronal response mechanisms. Unlike traditional methods such as least squares, Bayesian estimation adeptly handles the probabilistic nature of neuronal responses, offering robust analysis even with limited data and weak spatial selectivity. Through the analysis of both simulated and experimental data, we demonstrate that Bayesian estimation not only accurately fits the neuronal tuning curves but also effectively captures the nuances of both strongly and weakly selective neurons. Our results affirm the complex interdependencies among response parameters and highlight the variability in neuronal behavior under varied stimulus conditions. Our findings provide guidance as to how many response samples are necessary for Bayesian parameter estimation to achieve reliable fitting, making it particularly suitable for studies with constraints on data availability.

TABLE OF CONTENTS

LIST OF FIGURES

INTRODUCTION

Background on Primary Visual Cortex (V1)

The primary visual cortex (V1), a critical area in the brain's visual processing pathway, serves as the gateway for visual information entering the cortical regions. As the initial site for cortical visual processing, V1 neurons exhibit complex response patterns that encode various properties of visual stimuli. In early research on the receptive field of the visual cortex, it was found that neurons in the visual cortex of various mammals produce different responses to stimuli moving in different directionsHubel and Wiesel (1959, 1962). Some neurons generate a strong firing rate in response to striped stimuli moving in a specific directionHubel and Wiesel (1962); Wilson et al. (2018). Other neurons might respond to bars moving in either direction, such that they are selective for the bar orientation alone (for example, horizontal or vertical)Hubel and Wiesel (1968); Henry et al. (1974); Ohki et al. (2005). Therefore, V1 neurons can exhibit orientation selectivity and/or direction selectivity.

Orientational and Directional Selectivity

Orientation selectivity and directional selectivity refers to the ability of V1 neurons to respond preferentially to edges and bars of particular angle in space. These selectivities are not merely a result of the anatomical and synaptic organization of V1 but also involve dynamic aspects of neuronal processing, such as the temporal synchronization of neuronal firing and the interplay between excitatory and inhibitory neural inputs. Understanding these properties provides insights into the fundamental mechanisms of visual perception and has implications for broader applications such as artificial vision systems and the diagnosis of visual disorders. Among these, orientational and directional selectivity are fundamental for recognizing object edges and motion direction, which are crucial for navigation, pattern recognition, and behaviorally relevant decision-making.

Statistical Challenges in Analyzing Neuronal Data

Analyzing data from V1 presents unique challenges, primarily due to the variability and complexity of neuronal responses. Traditional statistical methods like least squares fitting have been extensively used to determine the parameters that best describe neuronal tuning curvesMazurek et al. (2014).However, least squares methods to not readily incorporate uncertainty in response properties. For example, if a vector parameter has an angle but the vector is small, the angle of the vector is highly uncertain. Least squares methods will produce a single angle measurement, whereas the uncertainty in the angle will be well captured in the probability distribution of the parameter. Bootstrap methods are invaluable for assessing the stability and reliability of the estimates derived from noisy data. By resampling the data and recalculating estimates numerous times, bootstrap methods help quantify the uncertainty in estimates, providing confidence intervals and validating the robustness of the modeling approachEfron and Tibshirani (1993).

Bayesian Parameter Estimation

Different from traditional methods, Bayesian estimation emerges as a powerful alternative by incorporating uncertainty and prior beliefs and continuously updating these beliefs in light of new evidence. This approach is particularly advantageous in neuroscience, where prior experimental results or physiological constraints provide a basis to form reasonable priorsCronin et al. (2010); Lewicki (1994). For instance, Bayesian methods can integrate existing knowledge about typical response shapes or expected noise levels to improve the robustness and accuracy of parameter estimation in the presence of sparse or noisy data.In this thesis, one of our goal is to establish a fundamental Bayesian analysis method without prior probabilities, to validate the feasibility and robustness of the Bayesian approach in analyzing visual neuronal response curves.

MATERIALS AND METHODS

Neurons generate spikes after being exposed to a stimuli. This signal depends on both the stimulus type and neurons typeDayan and Abbott (2005). The spiking frequency of neurons in the visual cortex exhibit spatial selectivity which includes direction and orientation tuning. When a stimulus, such as a long black bar, moves in different directions, neurons will produce different spike responses due to different moving directions and the inherent properties of the neurons themselves.

data collecting and simulating

In the laboratory, we used two-photon imaging of the calcium indicator dye Oregon Green Bapta-1 to measure responses of juvenile ferret visual cortex to stimuli moving in different directions Li et al. (2008). To test the model in this paper, a set of simulated data, which theoretically the same type as the laboratory data set, was used to evaluate the effectiveness of Bayesian analysis.

signal model

The neural cell response model we employ is expressed through a double Gaussian model with five parametersMazurek et al. (2014), and the formula is as follows:

$$Rsp(\theta) = C + R_{pref} * e^{-\frac{angdiff(\theta-\theta_{pref})^2}{2\sigma^2}} + R_{null} * e^{-\frac{angdiff(\theta-\theta_{null})^2}{2\sigma^2}} \tag{1}$$

Five parameters are included in the equation, which are C, R_{pref}, R_{null}, θ_{pref} and σ. θ_{pref} is the preferred direction. In direction space, the range of θ is $[0, 360^\circ)$, and $\theta_{null} = \theta_{pref} + 180^\circ$. To confine the movement direction within 360°, the function $angdiff = min(|\theta|, |\theta - 360|, |\theta + 360|)$ computes the absolute angular difference around the circle..In the response curve, σ is the standard deviation of Gaussian distribution. In general, offset,which is C, means the value of static frequency and background noise due to laboratory equipment and measurement. R_{pref} is the magnitude above the preferred direction offset and R_{null} is the magnitude above the null direction(opposite-preferred direction).

noise model

Noise can become variable and it's basically depending on which kind of detection technology is used. The noise in simulated data follows a Gaussian distribution with a mean equal to 50% of the response frequency in each direction. In other words, the noise in simulated data follows $X \sim N(Rsp(\theta), (0.5 * Rsp(\theta))^2)$Softky and Koch (1993). Laboratory data, collected through extracellular electrodes, exhibits noise with a tuning width σ linearly related to the reaction frequency in logarithmic spaceLi et al. (2008); Mazurek et al. (2014). To maintain consistency with the analysis of laboratory data, linear fitting in logarithmic space is employed to compute the tuning width σ of the noise in simulated data. The formula of noise tuning width is as follows:

$$log\sigma = C + S * logRsp(\theta)$$

$$\sigma = 10^C * Rsp(\theta)^S \tag{2}$$

data analysis

The movement direction in the context of direction selectivity need to be well defined. To facilitate comparison with the laboratory data mentioned in the paper, all data in this study are presented using 'compass' coordinates. Specifically, horizontal stimuli moving upward is considered to be moving at 0°, and angles increase in a clockwise manner. Meanwhile, Cartesian coordinate system is frequently used in other research. In Cartesian coordinate system, a vertical stimuli moving to the right is considered to be moving at 0°, and angles increase in a counterclockwise direction. The angle conversion formula between these two systems is as follows:

$$\theta_{cartesian} = 90^\circ - \theta_{compass}$$

Additionally, selectivity is categorized into orientation and direction. In direction space, the range of movement direction for stimuli is from 0° to 360°, whereas in orientation space, the range is limited from 0° to 180°. In the orientation space, the response frequency of stimuli in a particular direction and its opposite direction (back and forth) in direction space are averaged together.

Bayes' theorem is stated mathematically as the following equation:

$$P(H|D) = \frac{P(D|H)P(H)}{P(D)} \tag{3}$$

In the equation, H represents the hypothesized model $Rsp(\theta)$, which consists of five given parameters representing the theoretical response frequencies in a specific direction. D represents the numerical values of the responses from simulated or real data. $P(H|D)$ stands for the posterior probability, which is the probability of the model H being true given the observed data D. $P(D|H)$ is the likelihood function, representing the probability of observing data D given that the hypothesis is true. $P(H)$ is the prior probability, representing the probability distribution of hypotheses before considering the dataset. In this paper, it is assumed that there is no known probability adjustment for any hypothesized model, thus all prior probabilities of hypotheses are uniform distributions, i.e., constant. $P(D)$ is the model evidence, also known as the marginal distribution. Since the

same dataset is used across all possible hypotheses without any updates, $P(D)$ is constant in this paper. Therefore, there exists a proportional relationship between the posterior probability and the maximum likelihood $P(H|D) \propto P(D|H)$.

Bayesian treatment of orientation and direction tuning

OI (Orientation Index) and *DI* (Direction Index) are two indices of neuronal direction/orientation selectivity. Their magnitudes are used to characterize the sensitivity of neurons to stimuli motion in different directions/orientations in space. There are some differences in the definitions of these two index. In this paper, the index equations are as follows:

$$OI = (R_{pref} + R_{null} - (R_{orth+} + R_{orth-}))/(R_{pref} + R_{null}) \tag{4}$$

$$DI = (R_{pref} - R_{null})/R_{pref} \tag{5}$$

RESULTS

To evaluate the predictive accuracy and sensitivity of the Bayesian estimation model, we simulated response curves for two different types of cells and performed parameter estimation. All error bars in the text are represented using standard errors of the mean (SEM).

Bayesian estimation for simulated strong and weak spatial selectivity

As shown in **Figure 1**, multiple graphs illustrate the response characteristics of simulated neurons. The left column, labeled as "Well-tuned", features graphs that exhibit neuronal responses with higher peak firing rates and marked preferences for specific directions and orientations of stimuli. These responses are quantified in terms of frequency (Hz) and marginal likelihood across different orientations and directions, denoted by directional and orientation indexes. The right column, labeled as "Poorly-tuned", displays neurons with significantly lower response amplitudes, less distinct tuning curves, indicating a reduced selectivity for stimulus features. As shown in **Figure 1 A and Figure 1 B**, the black curves represent the ideal response curve of simulated data without any noise. To approximate real data more closely, we used simulated sampling points with an added 50% Gaussian noise for fitting. Each data point is based on five samples, covering a total of 36 angles. These sampling points are represented as blue dots in the figure. The noisy data, alongside results from a linear noise model, serve as inputs for Bayesian estimation, which are then interpolated based on given parameter ranges to produce the fits displayed as red curves. The parameter settings for the well-tuned simulated cells are ($C = 1$, $R_{pref} = 10$, $R_{null} = 5$, $\theta_{pref} = 90^\circ$, and $\sigma = 30^\circ$), while those for the poorly-tuned cells are ($C = 1$, $R_{pref} = 1$, $R_{null} = 0$, $\theta_{pref} = 90^\circ$, and $\sigma = 30^\circ$). The Bayesian fitting curves for both types of simulated cells closely align with the ideal curves, particularly for the well-tuned cells in terms of the preferred angle and tuning width values. **Figure 1 C, D, E** and **F** describe the marginal probability distributions for θ_{pref} and Response pref. The probability peaks accurately estimate the 'true values' of θ_{pref} and R_{pref}, and the model describes the reliability of the results through the probability distribution by its peaks and widths. Due to the poorly-tuned cells exhibiting weak spatial selectivity, the estimated probability for θ_{pref} is dispersed across various angles, resulting in a flatter spatial probability distribution compared to well-tuned cells. For R_{pref}, since both cell types are fitted within the same value range, and well-tuned cells with noise cover a broader sampling range, a more conservative R_{pref} probability distribution can be observed when fitting well-tuned cells. Conversely, smaller changes in sampling values correspond to a narrower estimated probability distribution. **Figure 1 G, H,**

I and **J** illustrates the probability distributions for the spatial selectivity index *DI* and *OI*. It can be observed that the well-tuned cells display distinct, singular probability peaks for DI and OI, accurately estimating the 'real' values ($OI = 0.86$, $DI = 0.45$). In contrast, for the poorly-tuned cells, both indices exhibit significant peaks near zero, although a close estimation to the 'real' value ($OI = 0.33$, $DI = 0.5$) is also observed in the probability distribution ($OI = 0.3$, $DI = 0.38$). In **Figure H and J**, for the fitting results of poorly-tuned cells, the presence of a peak at zero suggests that the cells are unlikely to exhibit spatial selectivity. Simultaneously, the occurrence of peaks at lower values and the distribution of the probability wave indicate the most likely value of *OI* and *DI* within the fitting range of parameters. This apparent contradiction of the index values in the fitting results could be due to the parameter ranges used not being optimal. There may be potential parameter combinations outside the chosen range that have not been included in the Bayesian estimation fitting process. This has resulted in probabilities outside the chosen range being accounted for in the probability estimates that approximately equal to zero.

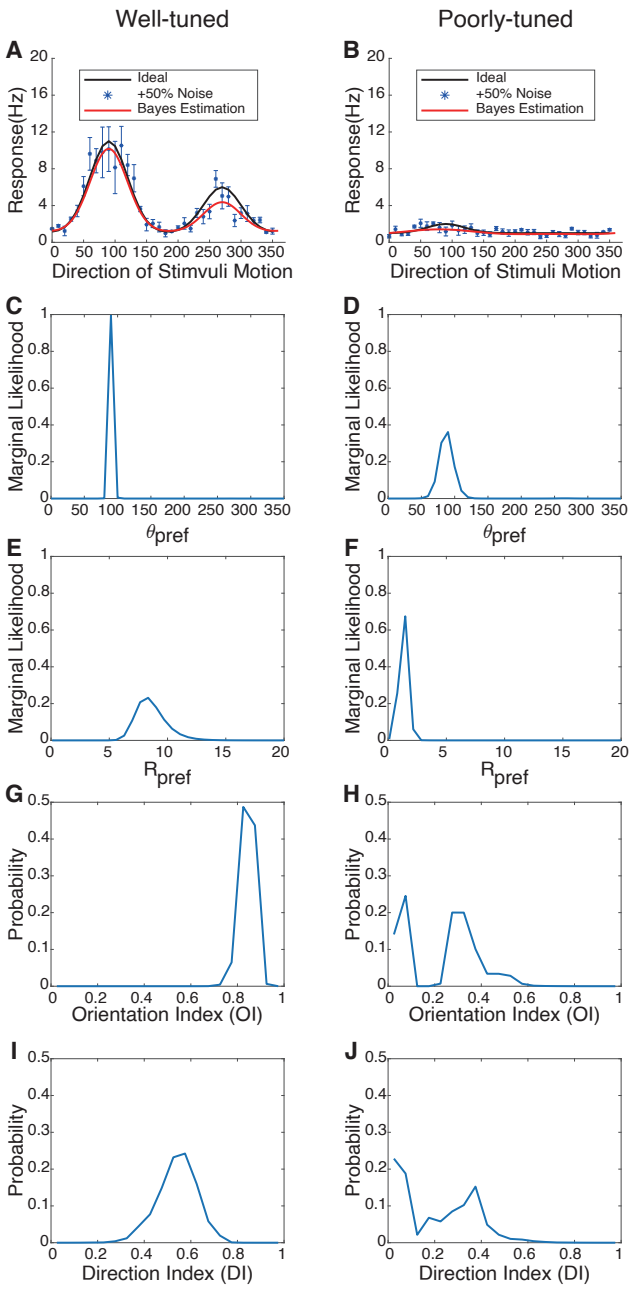

Figure 1: **Bayesian estimation for two types of simulated cells with different levels of tuning. (A & B)** Simulated response curve, data collection points with +50% Gaussian noise, and Bayesian estimation results. **(C & D & E & F)** The marginal likelihoods of θ_{pref} and R_{pref} in the model.**(G & H & I & J)** The probability distribution of *OI* and *DI* for spatial selectivity under Bayesian estimation.

Bayesian estimation for simulated temporal frequency

In numerous studies on the directional selectivity of the primary visual cortex, stimulus presentation in units of bars or cycles per second. For instance, the thickness of a striped stimulus represents a type of spatial frequency, while temporal frequency generally refers to the frequency of stimulus presentation. Neurons exhibit varying degrees of spatial selectivity at different temporal frequencies. The neurons with different temporal frequency properties come from unpublished work (Victor S. C. and Stephen V. H., unpublished observations)

In **Figure 1**, we initially explored the Bayesian estimation for fitting cells with different levels of directional selectivity. To further test the model's fitting efficacy in practical applications, in **Figure 2**, we simulated the changes in spatial selectivity of a single neuron under three different temporal frequencies,which are represented as high, medium, and low level. In our simulations, we hypothesized that the direction selectivity is strongest at low temporal frequency ($C = 1$, $R_{pref} = 7$, $R_{null} = 1$, $\theta_{pref} = 45^\circ$, and $\sigma = 30^\circ$). The maximum response amplitude is smaller at medium temporal frequency ($C = 1$, $R_{pref} = 5$, $R_{null} = 5$, $\theta_{pref} = 45^\circ$, and $\sigma = 30^\circ$), but the orientation selectivity is strongest at this setting. At high temporal frequency ($C = 1$, $R_{pref} = 0$, $R_{null} = 0$, $\theta_{pref} = 45^\circ$, and $\sigma = 30^\circ$), there is an absence of spatial selectivity. As shown in **Figure 2 A, B, C**, red represents the simulated sampling data points, blue curve represents the simulated ideal curve for low temporal frequency, yellow for medium temporal frequency, and green for high temporal frequency. To more closely replicate the actual fitting process, the number of sampling angles was reduced from 32 in **Figure 1** to 16. **Figure 2 D, E, F** shows the changes in the probability distributions of θ_{pref}, R_{pref}, and DI across the three different temporal frequencies, with the colors corresponding to the three temporal frequencies mentioned above. In **Figure 2 D**, Bayesian estimation accurately identifies the preferred angle at low temporal frequency. At medium temporal frequency, since the response rates at R_{pref} and R_{null} are nearly identical, the model indicates two closely matched probability peaks at θ_{pref} and θ_{null}. For high temporal frequency, the probability distribution lacks distinct peaks, suggesting that Bayesian estimation finds no significant spatial selectivity at this frequency. This is further supported in **Figures 2 E** and **F**, where the probability

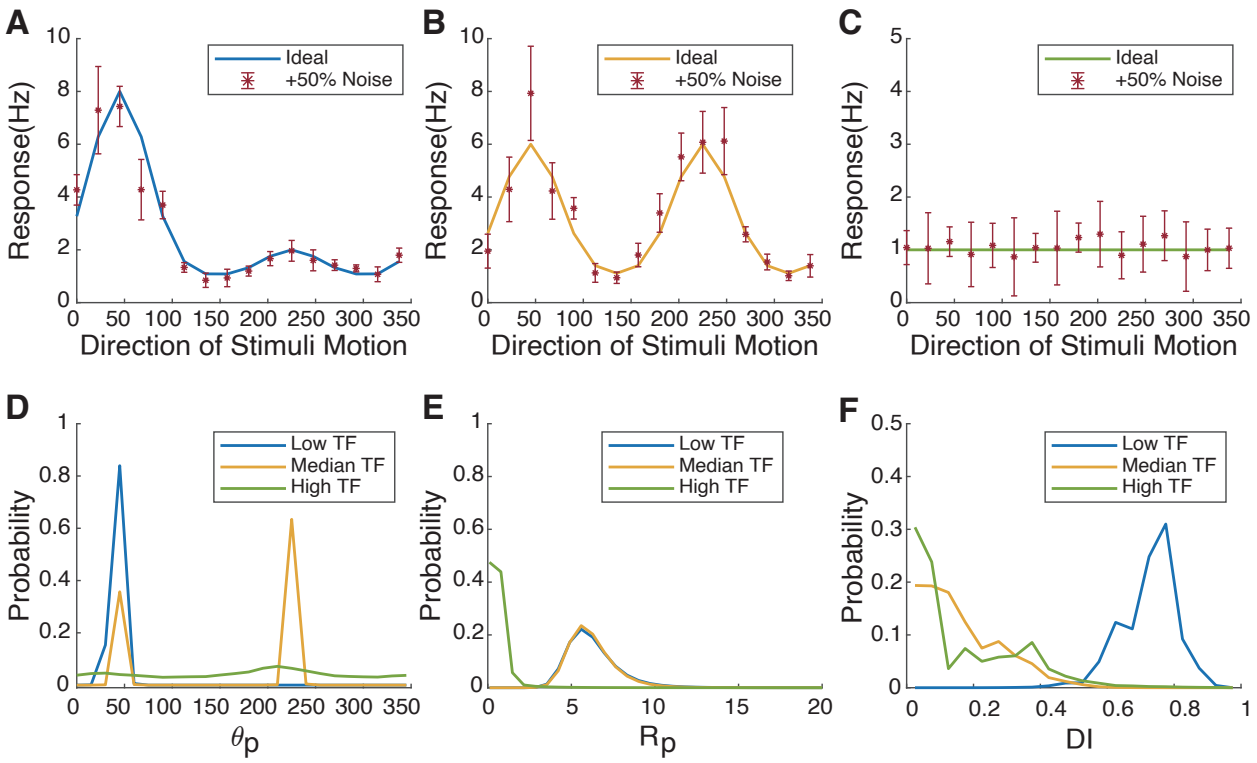

Figure 2: **Neuronal responses and Bayesian estimation to stimuli at different temporal frequencies in simulated cell(A & B & C)** Simulated 'real' response curves and sampling points with 50% added Gaussian noise in different temporal frequencies.**(D & E & F)** The probability distribution of θ_{pref}, R_{pref}, and DI fitted for different temporal frequencies.

peak of R_{pref} and DI at high temporal frequency predominantly cluster near or at zero, indicating minimal spatial selectivity. For medium temporal frequency, the obvious peak around 6 for R_{pref} and the peak near zero for DI suggest that the 'real' response curve has significant orientational selectivity with similar value of R_{pref} and R_{null}. The parameters and direction index for all three temporal frequencies successfully approximate the 'true values'.

Bayesian estimation fitting for simulated data with graded orientation index and direction index

To better test the universality and accuracy of Bayesian estimation, we simulated two groups of neurons, each consisting of five cells with gradually increasing *OI* and direction index *DI* values, ranging from 0 to 1. Additionally, to enhance the model's fitting speed and to assess the fitting outcomes with fewer samples, each simulated cell was tested at eight sampling angles.

Similarly, in **Figure 3** and **Figure 4**, the red color represents the sampling data, with each cell correspondingly represented by different colors.The legends in Figures 3 and 4 display the simulated true values of the *OI* and *DI*. In **Figure 3 A, B, C, D, E**, each color corresponds to the 'true' tuning curve of a simulated cell. Sampling on these curves, followed by the $+50\%$ noise, generates the sampling datasets. The black curve represents the fitting results. The fitting outcomes in **Figure 3 A, B** indicate that high response offsets and weak spatial selectivity can result in poor fitting results due to the randomness and noise of the sampling data. However, the probability distributions of some model parameters demonstrate the low reliability of using this dataset for fitting. For example, in **Figure 3 A**, the cell represented in blue with $OI = 0$, despite the fitted tuning curve showing a single distinct peak, there are no significant peaks in the R_{pref}, σ, and θ_{pref} probability distributions in **Figure 3 G, H, I**. Moreover, the highest probability for *OI* lies in the range from 0 to 0.05, yet there is a significant probability peak at high values for response offset. This probability distribution suggests that the reliability of the fitted curve is low, likely representing a cell with a high response offset but lacking orientational selectivity.A similar situation is observed with the cell represented by yellow in **Figure 3 B**. In the fitting results, there is a slight rightward shift in the probability distribution for *OI*, which indicates that the probability of the OI value is not zero but is relatively small. This aligns with the 'real' OI value of the yellow cell. As the response offset decreases and the OI values increase, the reliability of the model fitting improves. The probability distributions for various parameters exhibit distinct peaks, and the fitted curves consistently align with the true tuning curves of the simulated cells. Especially in **Figure 4**, throughout the process of *DI*increasing from 0 to 1, each parameter, including *DI*, exhibits at least

one distinct probability peak.

In **Figure 4**, all five simulated cells exhibit orientation selectivity, and each one simulates a tuning curve that has been adjusted to remove the response offset. It is evident that all parameters are able to accurately fit the 'real' values. Specifically, in **Figure 4 I**, for the cell represented in blue, where the R_{pref} and R_{null} are equal, the probability distribution for θ_{pref} shows two peaks that are nearly equal in height. In contrast, the cell represented in green more prefer one angle, while the other colors show only one probability peak. This phenomenon aligns with the graded changes in DI values. It is notable that in **Figure 3 I**, the θ_{pref} probability distributions for the five cells exhibit at most one peak. This is because all cells in Figure 3 have a DI value of 0.5, and cells with smaller OI values do not exhibit a probability peak for θ_{pref}. In contrast, because the five simulated cells in **Figure 4** all possess good orientational selectivity, each cell's θ_{pref} has at least one distinct probability peak. Meanwhile, a jagged curve change appears in the *DI* probability distribution. This may be due to the fact that the fitted DI values are calculated from multiple parameters, resulting in uneven distributions that cause some gaps in the final *DI* probability distribution. However, as shown in **Figure 4 F**, the gaps in the probability distribution do not affect the determination of the probability peak locations. The Bayesian estimation's DI fitting results still approximate the simulated 'real' values.

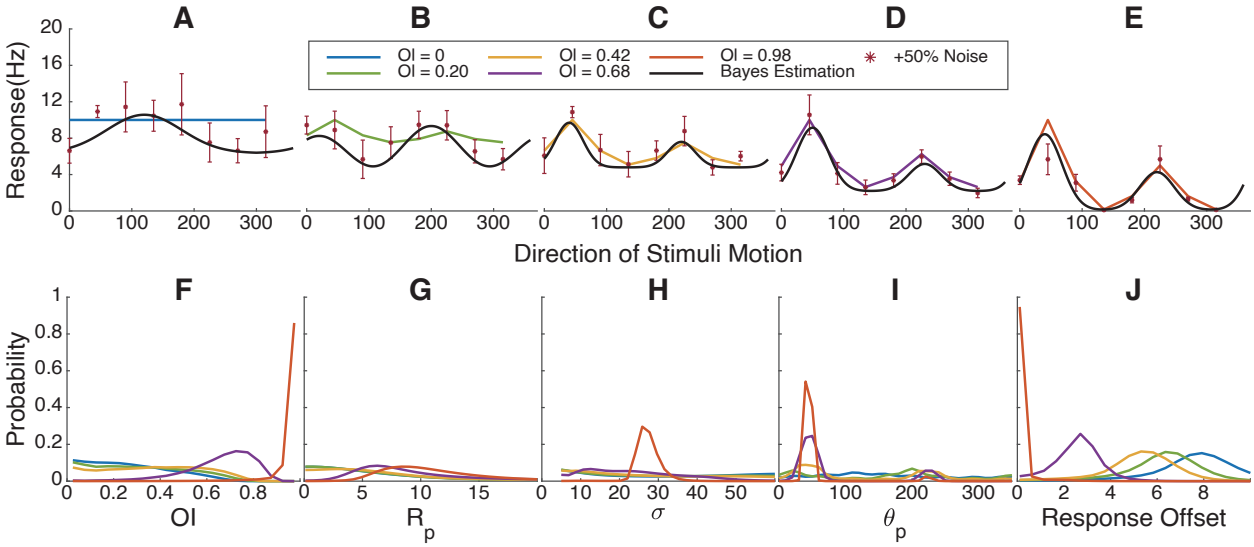

Figure 3: **Bayesian estimation results for simulated cells with gradually increasing orientation index values. (A & B & C & D & E)** Simulated response curve, sampling points with +50% Gaussian noise and fitting results. **(F & G & H & I & J)** The marginal likelihoods distribution of OI, R_{pref}, σ, θ_{pref} and C.

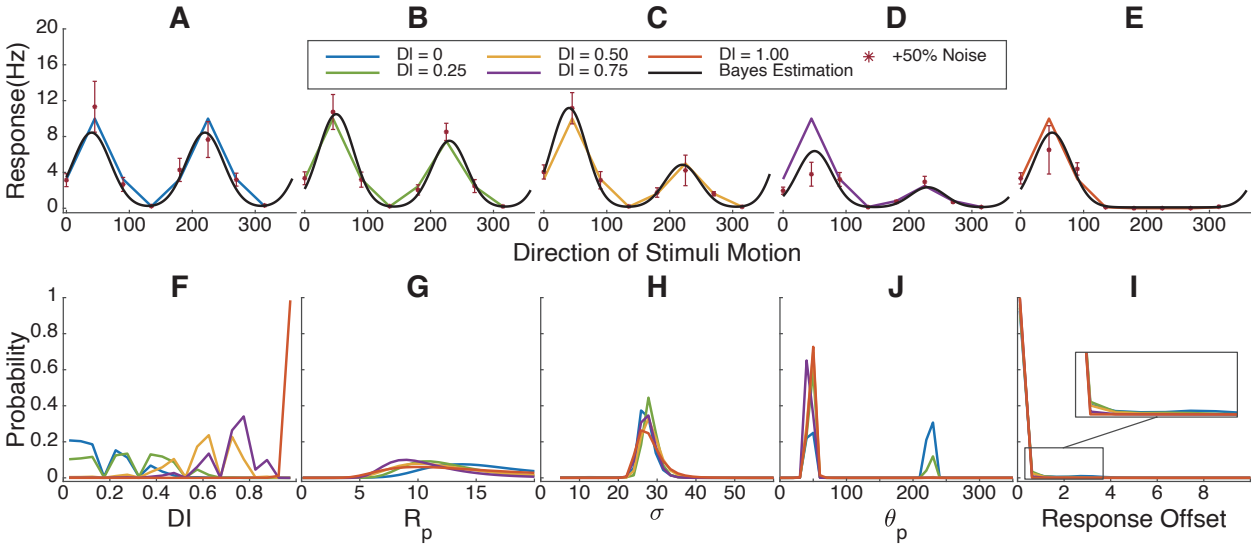

Figure 4: **Bayesian estimation results for simulated cells with gradually increasing direction index values. (A & B & C & D & E)** Simulated response curve, sampling points with +50% Gaussian noise and fitting results. **(F & G & H & I & J)** The marginal likelihoods distribution of DI, R_{pref}, σ, θ_{pref} and C.

Impact of Sampling Angle Quantity on Bayesian Estimation Fitting Results

In the actual process of collecting firing rates from ferret neurons, a substantial amount of data may be unusable, while the number of sampling angles and the quantity of data collected are limited by the duration of the experiment and the capabilities of the hardware. For any data fitting method, it's essential to be able to handle limited input data effectively. It can take considerable time to present stimuli and collect stimulus response from neurons, so it is important to understand how many stimulus repetitions might be needed to provide a reasonable Bayesian parameter estimation. To determine the minimum requirements needed for Bayesian estimation to achieve reliable fitting results, we further explored the impact of different sampling angle quantities on Bayesian estimation using simulated tuning curves.

Each color in the **figure 5** corresponds to a different number of sampling angles, with the legend indicating the number of angles used for each Bayesian estimation fitting. The parameters of the simulated tuning curve are set as ($C = 2.5$, $R_{pref} = 7.5$, $R_{null} = 3.75$, $\theta_{pref} = 45^\circ$, and $\sigma = 30^\circ$). From the probability distribution of OI in **Figure 5 F**, it can be observed that four sampling angles are insufficient to produce a good fitting curve. There is also a significant likelihood of obtaining a fit with low spatial selectivity due to the accidental collection of angles where the response frequency in the 'real' tuning curve is lower. Starting from eight sampling angles, a probability peak can be seen around 0.6, although it is somewhat flat. Similarly, in **Figures 5 G J**, higher sampling angles concentrate the probability peaks at specific values, and the fitting curves align well with the 'real' tuning curve. This indicates that eight or more sampling angles meet the minimum requirements for Bayesian estimation. However, under this parameter set, the probability distribution for σ remains flat, with an indistinct peak in the range from 20 to 30. This is consistent with the results observed in **Figures 3 H** and **Figure 4 H**. In these cases, where the parameter distributions are flat, the response offset is not zero. Nevertheless, **Figure 5 I** shows good fitting for the response offset across all sampling angle quantities.

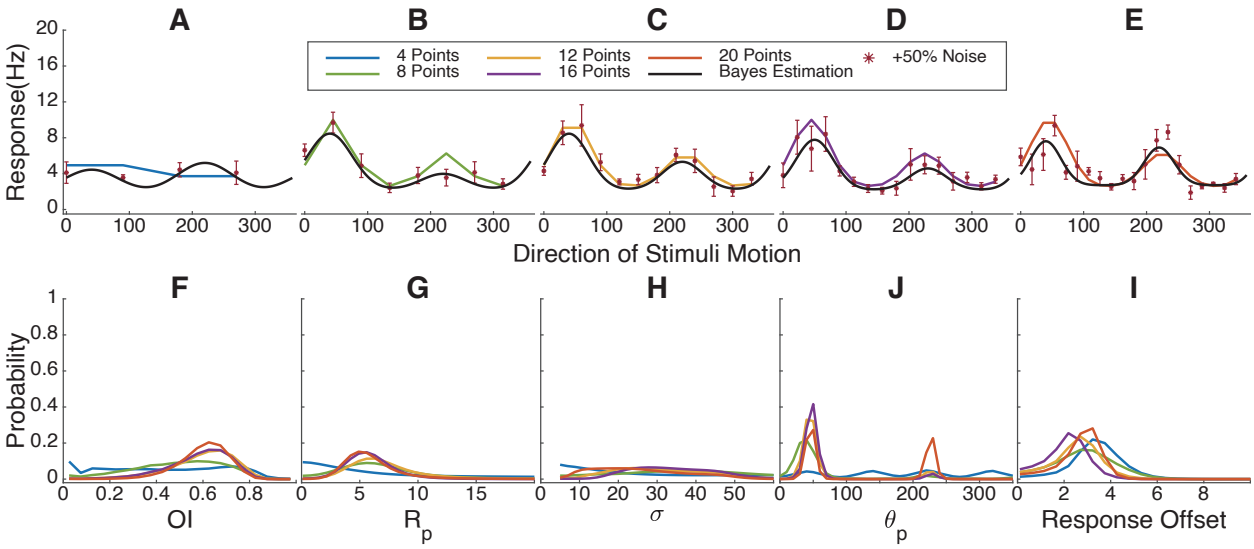

Figure 5: **Impact of varying sampling angle quantities on Bayesian estimation results. (A & B & C & D & E)** Simulated response curve, sampling points with +50% Gaussian noise and fitting results.**(F & G & H & I & J)** The marginal likelihoods distribution of OI, R_{pref}, σ, θ_{pref} and C.

Bayesian Estimation Fitting Results for Neuronal Response Curves in the Ferret Primary Visual Cortex

After employing simulated neurons with varying levels of orientational selectivity and directional selectivity, as well as exploring the impacts of different input parameters and variables such as sampling angles, we proceeded to collect response tuning curves of primary visual cortex neurons from adult ferrets using calcium imaging. We then applied Bayesian estimation to fit the data. Unlike the simulated data, the actual experimental data yields relative fluorescence intensity, $\delta F/F$, which corresponds to the response frequency (Hz) in the simulated tuning curves. Due to significant changes in numerical ranges, this require adjustments in the fitting value ranges for R_{pref} and C within the Bayesian estimation model.

After an initial screening, we identified neurons in the dataset that may exhibit orientational or directional selectivity and selected the first five as cases for Bayesian estimation fitting. As shown in **Figure 6 A, B, C, D, E**, each color corresponds to a cell, and the curves represent the maximum likelihood fitting curves. In **Figure 6 J**, it is notable that all cells have similar preferred angles, suggesting that this group of cells is likely collected from the same region. Additionally, **Figure 6 I** shows that the response offsets of the cells are essentially the same. In **Figure 6 G**, the probability distribution of R_{pref} lies between 0 to 0.1, with the green and purple cells showing smaller R_{pref} values. Considering the OI and σ probability distributions in **Figures 6 F H**, the green and purple cells likely exhibit weaker orientational selectivity.

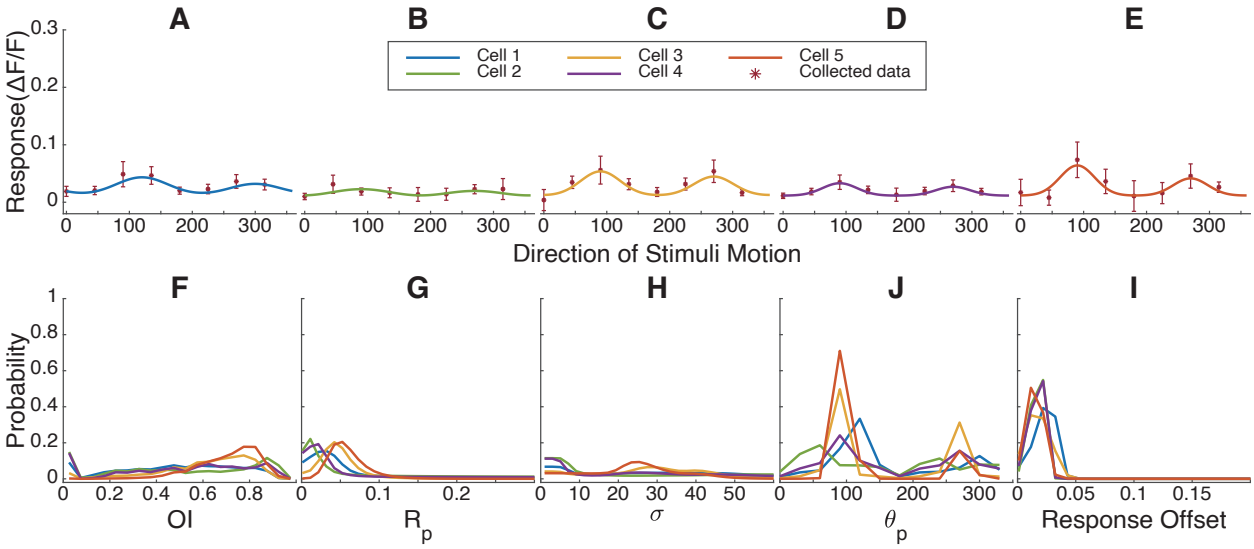

Figure 6: **Impact of varying sampling angle quantities on Bayesian estimation results. (A & B & C & D & E)** The response of juvenile ferret visual cortex to stimuli moving in different directions and Bayesian parameter estimation results. **(F & G & H & I & J)** The marginal likelihoods distribution of OI, R_{pref}, σ, θ_{pref} and C.

DISCUSSION

The observed flattening of the probability distributions for certain parameters when there is a high response offset could be due to the interdependence among parameters. Parameters in a model, especially in a complex system like neural responses, often interact with each other. This interdependence means that changes in one parameter can affect the values and distributions of others. This lack of independence complicates the fitting process and can disturb the estimation results. When using Bayesian estimation, considering the relationships between parameters, such as their potential correlations or interactions, is crucial for accurate modeling. It may be necessary to adjust the model to account for these dependencies, possibly through a hierarchical or multi-level Bayesian approach, and to integrate it with prior probabilitiesLewicki (1994); Cronin et al. (2010), which can better handle the complex interactions between parameters. Further analysis and modeling strategies that incorporate these interdependencies could lead to more robust and reliable estimation results.

The probability distributions of the fitting results currently depend heavily on the fitting range and quantity of each parameter. Inappropriate fitting ranges can cause an increase in the probability distributions of some parameters and selectivity indices near zero, and also reduce the height of the probability peaks. This can misrepresent the underlying neural properties by suggesting a lack of selectivity where there might be significant neural behavior.

Comparing the bootstrap results with actual dataLi et al. (2008), the Bayesian estimation fitting results show slight shifting, even though the values are still close. This drift might be caused by the errors introduced by the Gaussian noise model used in the analysis. Further investigation is needed to explore the reasons behind this drift. Analyzing the impact of the noise model on the fitting results could help refine the estimation process and improve accuracy. It's essential to understand how different noise levels and types influence the Bayesian estimation to ensure that the model assumptions align with the actual data characteristics.

REFERENCES

B. Cronin, I.H. Stevenson, M. Sur, and K.P. Körding. Hierarchical Bayesian modeling and Markov chain Monte Carlo sampling for tuning-curve analysis. *J Neurophysiol*, 103:591–602, 01 2010. ISSN 0022-3077. doi: 10.1152/jn.00379.2009.

Peter Dayan and L. F. Abbott. *Theoretical Neuroscience: Computational and Mathematical Modeling of Neural Systems*. The MIT Press, 2005. ISBN 0262541858.

Bradley Efron and Robert J. Tibshirani. *An Introduction to the Bootstrap*. Number 57 in Monographs on Statistics and Applied Probability. Chapman & Hall/CRC, Boca Raton, Florida, USA, 1993.

G H Henry, B Dreher, and P O Bishop. Orientation specificity of cells in cat striate cortex. *Journal of Neurophysiology*, 37(6):1394–1409, 1974. doi: 10.1152/jn.1974.37.6.1394. URL https://doi.org/10.1152/jn.1974.37.6.1394. PMID: 4436709.

D. H. Hubel and T. N. Wiesel. Receptive fields of single neurones in the cat's striate cortex. *The Journal of Physiology*, 148(3):574–591, 1959. doi: https://doi.org/10.1113/jphysiol.1959.sp006308. URL https://physoc.onlinelibrary.wiley.com/doi/abs/10.1113/jphysiol.1959.sp006308.

D. H. Hubel and T. N. Wiesel. Receptive fields, binocular interaction and functional architecture in the cat's visual cortex. *The Journal of Physiology*, 160(1):106–154, 1962. doi: https://doi.org/10.1113/jphysiol.1962.sp006837. URL https://physoc.onlinelibrary.wiley.com/doi/abs/10.1113/jphysiol.1962.sp006837.

D. H. Hubel and T. N. Wiesel. Receptive fields and functional architecture of monkey striate cortex. *The Journal of Physiology*, 195(1):215–243, 1968. doi: https://doi.org/10.1113/jphysiol.1968.sp008455. URL https://physoc.onlinelibrary.wiley.com/doi/abs/10.1113/jphysiol.1968.sp008455.

Michael S. Lewicki. Bayesian Modeling and Classification of Neural Signals. *Neural Computation*, 6(5):1005–1030, 09 1994. ISSN 0899-7667. doi: 10.1162/neco.1994.6.5.1005. URL https://doi.org/10.1162/neco.1994.6.5.1005.

Ye Li, Stephen D. Van Hooser, Mark Mazurek, Leonard E. White, and David Fitzpatrick. Experience with moving visual stimuli drives the early development of cortical direction selectivity. *Nature*, 456:952–956, 2008. doi: https://doi.org/10.1038/nature07417. URL https://www.nature.com/articles/nature07417#citeas.

Mark Mazurek, Marisa Kager, and Stephen D. Van Hooser. Robust quantification of orientation selectivity and direction selectivity. *Frontiers in Neural Circuits*, 8, 2014. ISSN 1662-5110. doi: 10.3389/fncir.2014.00092. URL https://www.frontiersin.org/articles/10.3389/fncir.2014.00092.

Kenichi Ohki, Sooyoung Chung, Yeang H. Ch'ng, Prakash Kara, and R. Clay Reid. Functional imaging with cellular resolution reveals precise micro-architecture in visual cortex. *Nature*, 433:597–603, 2005. doi: 10.1038/nature03274.

WR Softky and C Koch. The highly irregular firing of cortical cells is inconsistent with temporal integration of random epsps. *Journal of Neuroscience*, 13(1):334–350, 1993. ISSN 0270-6474. doi: 10.1523/JNEUROSCI.13-01-00334.1993. URL https://www.jneurosci.org/content/13/1/334.

Daniel E Wilson, Benjamin Scholl, and David Fitzpatrick. Differential tuning of excitation and inhibition shapes direction selectivity in ferret visual cortex. *Nature*, 560(7716):97—101, August 2018. ISSN 0028-0836. doi: 10.1038/s41586-018-0354-1. URL https://europepmc.org/articles/PMC6946183.